UDC 539.4

On Issue of Comparison of the Unified Curve and Master Curve Methods and Application for RPV Structural Integrity Assessment

B. Z. Margolin, V. N. Fomenko, A. G. Gulenko, V. I. Kostylev, and V. A. Shvetsova

Central Research Institute of Structural Materials "Prometey", Saint-Petersburg, Russia

УДК 539.4

К вопросу сравнения методов Unified Curve и Master Curve и их применения к определению конструкционной прочности корпусов реакторов

Б. З. Марголин, В. Н. Фоменко, А. Г. Гуленко, В. И. Костылев, В. А. Швецова

ЦНИИ КМ "Прометей", Санкт-Петербург, Россия

Проанализированы два инженерных метода – Master Curve и Unified Curve применительно к оценке сопротивления хрупкому разрушению корпусов реакторов. Для сравнения этих методов при обработке базы данных по вязкости разрушения для 44 сталей и их швов с различной степенью охрупчивания было использовано три разных статистических параметра. Установлено, что метод Unified Curve имеет преимущества перед методом Master Curve. Проанализированы возможные причины кажущегося преимущества метода Master Curve, а также сформулированы и обоснованы требования для объективного сравнения методов. Обобщение экспериментальных данных по температурной зависимости термоактивированной части предела текучести и модели Prometey (модели хрупкого разрушения, основанной на локальном подходе) позволило объяснить, почему зависимость $K_{JC}(T)$ для различных сталей, при небольшой степени охрупчивания, может быть аппроксимирована экспоненциальной функцией, в частности зависимостью Master Curve. Получена корреляция между температурной зависимостью термоактивированной части предела текучести и зависимостью Master Curve.

Ключевые слова: конструкционная прочность корпуса реактора, трещиностойкость, Master Curve, Unified Curve, модель Prometey.

Introduction. At present, there are two engineering methods, namely, the Master Curve [1, 2] and the Unified Curve [3], that allow the construction of $K_{JC}(T)$ curve for different structural steels. Both methods use the Weibull statistics to describe the scatter in K_{JC} results and the effect of specimen thickness on $K_{JC}(T)$ curve. To describe the $K_{JC}(T)$ curves for embrittled material the Master Curve (MC) uses the lateral temperature shift concept, i.e., assumption about an invariance of the shape of the $K_{JC}(T)$ curve for different conditions of a material. The Unified Curve (UC) provides a prediction of the $K_{JC}(T)$ curve allowing for the possibility of shift of $K_{JC}(T)$ curve to higher temperature range and a variation in the $K_{JC}(T)$ curve shape. By other words, the UC, as distinct from the MC, takes into account the transformation of the shape of the $K_{JC}(T)$ curve as a function of the degree of embrittlement of a material.

Quantitative comparison of the MC and UC was performed for the first time in [3] and at a later date in [4] as applied for various ferritic steels with various degrees of embrittlement. For quantitative assessment the statistical parameters δ and σ have been used that are defined as follows.

The parameter δ is the root-mean-square deviation calculated by equation [3, 4]

$$\delta = \sqrt{\frac{1}{M}\sum_{j=1}^{M}(K_{JC(med)j}^{pr} - K_{JC(med)j}^{exp})^2}, \quad (1)$$

where M is the number of temperatures at which tests were carried out, $K_{JC(med)j}^{pr}$ is the predicted median value of K_{JC} calculated by the MC or UC at test temperature T_j, and $K_{JC(med)j}^{exp}$ is the median value of K_{JC} determined by treatment of experimental data at $T = T_j$ with the maximum likelihood method according to [1].

According to [1] $K_{JC(med)}^{exp}$ is calculated with formulae

$$K_{JC(med)}^{exp} = K_{\min} + (K_0 - K_{\min})[\ln(2)]^{1/4}, \quad (2)$$

$$K_0 = \left[\sum_{i=1}^{N}(K_{JCi}^{exp} - K_{\min})^4 / r\right]^{1/4} + K_{\min}, \quad (3)$$

where N is the number of specimens tested at $T = T_j$, r is the number of valid specimens tested at $T = T_j$, $K_{\min}$ is minimum value of fracture toughness that is taken according to [1, 2] as $K_{\min} = 20$ MPa$\sqrt{\text{m}}$, and K_{JCi}^{exp} is experimental K_{JC} value for *i*th specimen.

The parameter σ is calculated as [4]

$$\sigma = \sqrt{\frac{1}{N}\sum_{i=1}^{N}(K_{JC(mean)i}^{pr} - K_{JCi}^{exp})^2}, \quad (4)$$

where N is the total number of tested specimens, K_{JCi}^{exp} is experimental K_{JC} value for *i*th specimen, and $K_{JC(mean)i}^{pr}$ is the predicted mathematical expectation of K_{JC} calculated by the MC or UC at test temperature for *i*th specimen. Using the Weibull function for the K_{JC} distribution the $K_{JC(mean)i}^{pr}$ value may be calculated by formula [5]

$$K_{JC(mean)i}^{pr} = \frac{K_{JC(med)i}^{pr} - K_{\min}}{(\ln 2)^{1/4}}\Gamma\left(1+\frac{1}{4}\right) + K_{\min}, \quad (5)$$

where Γ is gamma function.

Thus, the parameters δ and σ may be used for quantitative comparison of the experimental and predicted $K_{JC}(T)$ curves. The parameter δ may be used when the number of specimens tested at temperature T_j is many enough so that $K_{JC(med)j}^{exp}$ may be reliably determined for each test temperature. If the number of tested specimens is less than necessary then the parameter σ should be used. It is necessary to note that the parameter σ differs from the parameter δ. If the prediction coincides with experiment completely then $\delta = 0$ but $\sigma \neq 0$. Nevertheless both the parameter δ and σ reduce when the predicted results are approaching to the experimental data.

For quantitative comparison of the MC and UC the ratios δ_{MC}/δ_{UC} and σ_{MC}/σ_{UC} may be used as the comparison tests. If $\delta_{MC}/\delta_{UC} > 1$ or $\sigma_{MC}/\sigma_{UC} > 1$ then the UC describes the experimental data more adequately than the MC. If $\delta_{MC}/\delta_{UC} < 1$ or $\sigma_{MC}/\sigma_{UC} < 1$ then the MC describes the experimental data more adequately than the UC.

Quantitative comparison of the MC and UC on the basis of the statistical parameters δ and σ has been performed in [3, 4] for various ferritic steels with various degrees of embrittlement. The results of comparison are represented in Fig. 1.

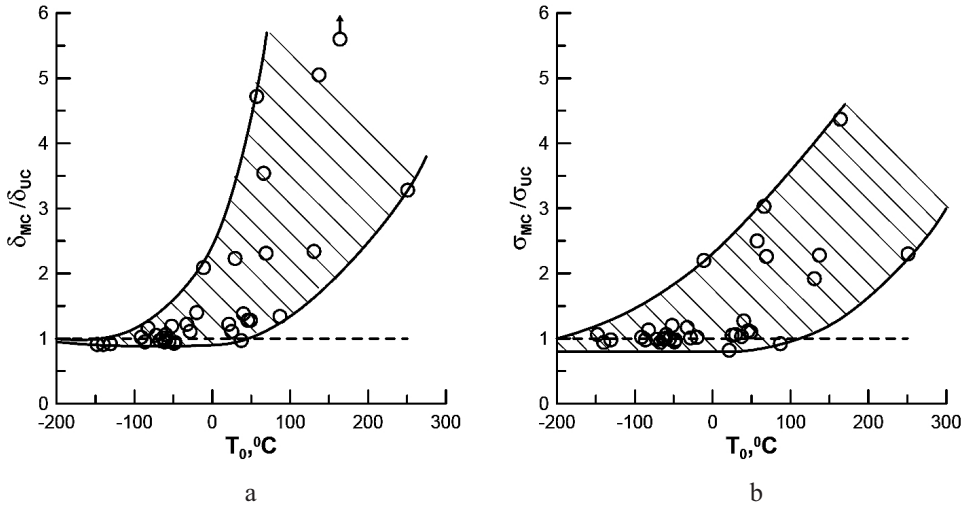

Fig. 1. Comparison of the MC and UC with the parameters δ and σ: the ratios δ_{MC}/δ_{UC} (a) and σ_{MC}/σ_{UC} (b) vs the reference temperature T_0 [4].

It is seen from Fig. 1 that for low values of T_0 (materials in the initial (as-received) condition and with small degrees of embrittlement) the $K_{JC}(T)$ curves predicted with the UC and MC are very close, and one method has not preference to another. When the value T_0 increases the description of $K_{JC}(T)$ by the UC becomes more adequate than the description by the MC as the UC takes into account a variation of the $K_{JC}(T)$ curve shape.

One more statistical parameter was used recently in [6] for quantitative comparison of the MC and UC. This is the parameter L that follows from the maximum likelihood method. (The parameters T_0 and Ω in the MC and UC are calibrated with the maximum likelihood method.)

The parameter L is calculated by formula [6]

$$L = \prod_{i=1}^{N} \frac{4(K_{JCi}^{exp} - K_{\min})^{3\delta_i}}{(K_0^{pr} - K_{\min})^{4\delta_i}} \exp\left(-\left\{\frac{K_{JCi}^{exp} - K_{\min}}{K_0^{pr} - K_{\min}}\right\}^4\right), \qquad (6)$$

where $\delta_i = 1$ for valid data and $\delta_i = 0$ for censored data, $K_0^{pr} - K_{\min} = (K_{JC(med)}^{pr} - K_{\min})[\ln(2)]^{-1/4}$ with $K_{JC(med)}^{pr}$ calculated with the MC or UC. (The other parameters are as above.)

When using the maximum likelihood method the most adequate $K_{JC}(T)$ curve corresponds to the maximum value of the parameter L. It means that the parameter L may be used for quantitative comparison of the experimental and predicted $K_{JC}(T)$ curves. The parameter L calculated by Eq. (6) is designated for the MC as L^{MC} and for the UC as L^{UC}.

For quantitative comparison of the MC and UC it is necessary to compare L^{MC} and L^{UC}: if $L^{UC} > L^{MC}$ then the UC describes the experimental data more adequately than the MC. If $L^{UC} < L^{MC}$ then the MC describes the experimental data better than the UC.

In [6] the difference $\ln L^{MC}/r - \ln L^{UC}/r$ is used as the comparison tests of the MC and UC. For short let's designate this difference as

$$Z \equiv \frac{\ln L^{MC}}{r} - \frac{\ln L^{UC}}{r}. \tag{7}$$

So, if $Z < 0$ then the UC describes the experimental data more adequately than the MC. If $Z > 0$ then the MC describes the experimental data better than the UC.

The results of comparison the MC and UC with the parameter L obtained in [6] are represented in Fig. 2. On the basis of these results the conclusion has been drawn in [6] that the MC describes the considered experimental data better than the UC. The considered data base consists of 50 sets and includes, in part, those considered in [3, 4].

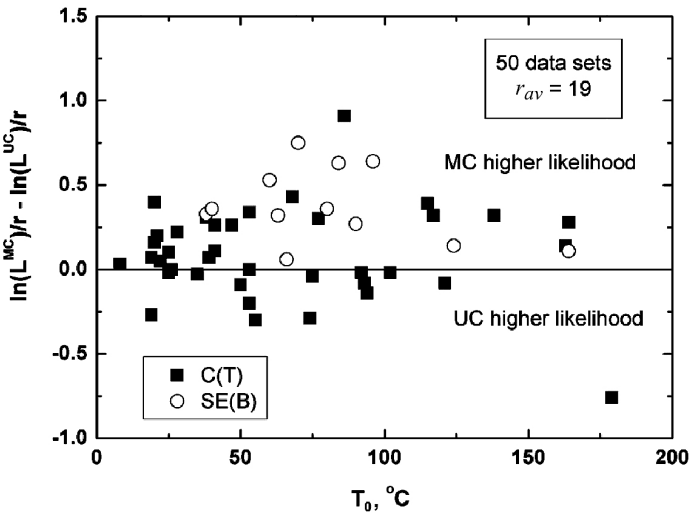

Fig. 2. Comparison of the MC and UC with the parameters L for the data sets from CT and SE(B) specimens according to [6].

Thus, it would be concluded that application of various statistical parameters for quantitative comparison of the MC and UC results in quite different and contradictory conclusions as in [3, 4] and in [6].

Additionally, Wallin [6] has declared that the parameter L or $\ln L/r$ provides more objective comparison as compared with the parameters δ and σ.

Thus, the main purposes of the present paper are (i) to compare the UC and MC with three statistical parameters L, δ, and σ, and (ii) to reveal possible reasons of contradictory conclusions in [3, 4] and in [6]. The paper considers also some important issues for justification of the Unified Curve and Master Curve methods.

1. **The Main Considerations of the Master Curve and Unified Curve Methods**. The main considerations of the Master Curve and Unified Curve methods are as follows.

1. The temperature dependence of fracture toughness at the fracture probability $P_f = 0.5$ for specimens with thickness $B = 25$ mm for any degree of embrittlement is described by the following equations.

According to the Master Curve [1]

$$K_{JC(med)}(T) = K_{JC}^{shelf} + \beta \exp(\gamma(T - T_0)), \qquad \text{MPa}\sqrt{\text{m}}, \tag{8}$$

where T_0 is the reference temperature in °C for which $K_{JC(med)}(T_0) = 100\,\text{MPa}\sqrt{\text{m}}$, T is temperature in °C, the numerical coefficients K_{JC}^{shelf}, β, and γ are fixed and taken as $K_{JC}^{shelf} = 30\ \text{MPa}\sqrt{\text{m}}$, $\beta = 70\ \text{MPa}\sqrt{\text{m}}$, and $\gamma = 0.019$.

According to the Unified Curve [3]

$$K_{JC(med)}(T) = K_{JC}^{shelf} + \Omega\left(1 + \tanh\left(\frac{T - 130}{105}\right)\right), \qquad \text{MPa}\sqrt{\text{m}}, \tag{9}$$

where $K_{JC}^{shelf} = 26\,\text{MPa}\sqrt{\text{m}}$, Ω is a constant for a given condition of a material, and T is temperature in °C.

2. The brittle fracture probability P_f for a cracked specimen with reference thickness $B = 25$ mm is described by the Weibull distribution function [1, 7]

$$P_f = 1 - \exp\left[-\left(\frac{K_{JC} - K_{\min}}{K_0 - K_{\min}}\right)^4\right], \tag{10}$$

where P_f is the fracture probability of a cracked specimen arbitrarily taken from the considered set at $K_J \le K_{JC}$ (K_J is the stress intensity factor), K_0 is a scale parameter depending on the test temperature and specimen thickness, and $K_{\min} = 20\ \text{MPa}\sqrt{\text{m}}$ in accordance with [1, 2, 8].

3. The effect of specimen thickness on fracture toughness for a fixed fracture probability is described by equation [1, 8]

$$\frac{K_{JC}^{X} - K_{\min}}{K_{JC}^{Y} - K_{\min}} = \left(\frac{B_Y}{B_X}\right)^{1/4}, \tag{11}$$

where K_{JC}^{X} and K_{JC}^{Y} are fracture toughness values for specimens with thicknesses B_X and B_Y at the same fracture probability.

4. To obtain $K_{JC}(T)$ curve for the embrittled materials the MC assumes that the only parameter, T_0, varies, and the UC assumes that the parameter Ω varies only. When degree of material embrittlement increases the T_0 value increases, and the Ω value decreases. Other numerical parameters in Eqs. (8) and (9) are fixed.

The parameter T_0 in the MC and the parameter Ω in the UC are calibrated by the maximum likelihood method on the basis of test results at one temperature (single temperature method) or at several temperatures (multi-temperature method). Requirements for the number and size of fracture toughness specimens are the same for both methods.

It is appropriate to give here some comments for the above considerations.

Equations (10) and (11) follow from the pioneer paper of the Beremin group [9]. It should be noted that a relation $P_f \sim K^4$ in Eq. (10) with the exponent value being equal to 4 does not depend on a local fracture criterion used, and the only condition (in addition to the Weibull statistics and the weakest link theory) is required to deduce this relation, namely, the condition of self-similarity (homothety) of stress-and-strain fields in plastic zone near a crack tip [9, 10]. (This issue is considered in detail in Section 3.)

The numerical coefficients β, γ, and K_{JC}^{shelf} in the MC [see Eq. (8)] were found from a best fit to experimental data sets for ferritic steels [2].

The numerical coefficients in the UC [see Eq. (9)] were found from a best fit to the $K_{JC}(T)$ curves calculated with the probabilistic model (known as the Prometey model) with the model parameters being typical for RPV steels in various conditions [3].

As it follows from consideration 4 the transformation of $K_{JC}(T)$ curve predicted with the MC and UC for the irradiated (embrittled) materials occurs in different manners. When degree of material embrittlement increases a lateral shift of the $K_{JC}(T)$ curve occurs according to the MC to an elevated temperature range. It means that the shape of the $K_{JC}(T)$ curve is the same for different conditions of a material. This transformation is illustrated by Fig. 3a.

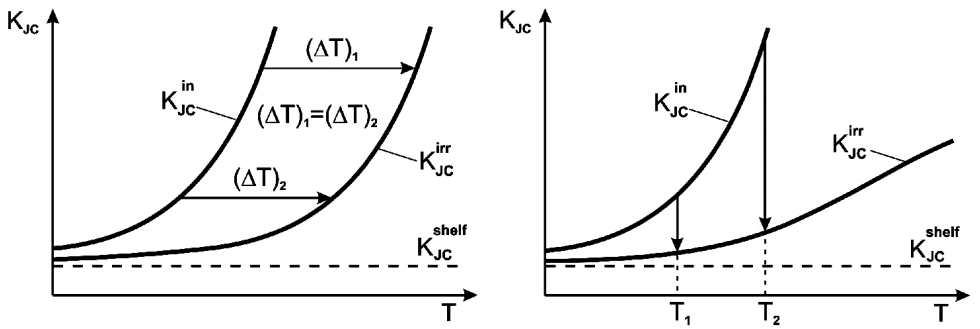

a b

Fig. 3. Transformation of $K_{JC}(T)$ curve for the irradiated materials according to the MC (a) and UC (b).

According to the UC for the irradiated (embrittled) materials a vertical evolvent of the $K_{JC}(T)$ curve occurs by such way that the value $[K_{JC}(T) - K_{JC}^{shelf}]$ decreases by the same factor Ω^{in}/Ω^{irr} (here Ω^{in} and Ω^{irr} are the values of Ω for initial and irradiated materials, respectively) for any temperature from the brittle fracture temperature range. This transformation is shown in Fig. 3b and clearly seen from Eq. (9) rewritten in the form

$$K_{JC}(T) - K_{JC}^{shelf} = \Omega f(T), \tag{12}$$

where

$$f(T) = \left(1 + \tanh\left(\frac{T-130}{105}\right)\right).$$

Thus, the standard Master Curve assumes that the shape of the $K_{JC}(T)$ curve is the same for different conditions of a material. The Unified Curve approximates the $K_{JC}(T)$ curve allowing for a possibility of a variation in the shape.

2. **Quantitative Comparison of the MC and UC with Various Statistical Parameters**. Comparison of the experimental fracture toughness data and $K_{JC}(T)$ curves predicted with the MC and UC has resulted in quite different and contradictory conclusions in [3, 4] and in [6]. One from possible reasons may consist in the using of different statistical parameters for comparison. In [3, 4] the parameters δ and σ were used as calculated by Eqs. (1) and (4), and in [6] the comparison was based on Eq. (7) with the L parameter.

To consider this reason we apply all three parameters for the fracture toughness data sets used in [3, 4].

The results of application of the parameters δ, σ, and L are represented in Table 1 for the data sets used previously in [3, 4]. The results of comparison of the MC and UC with the L parameter are shown in Fig. 4. It may be seen from Fig. 4 that the UC has advantage as compared with the MC for the considered data sets. This conclusion is in agreement with the conclusion based on application of the parameters δ and σ (see Fig. 1).

Table 1

The Results of Treatment of the Data Base Used in [3, 4] with Three Statistical Parameters (L, δ, and σ)

No.	Material	σ_Y at $T = 20$℃, MPa	T_0, ℃	Ω, MPa$\sqrt{\text{m}}$	Z	$\frac{\delta_{MC}}{\delta_{UC}}$	$\frac{\sigma_{MC}}{\sigma_{UC}}$	Reference
1	2	3	4	5	6	7	8	9
1	A533B steel (in)	567	−148.0	7397	0.02	0.91	1.06	[11]
2	A508 steel (in)	650	−140.0	6441	−0.04	0.91	0.94	[11]
3	HY130L (in)	955	−131.0	5405	−0.01	0.92	0.98	[11]
4	ABS DS (in)	270	−91.3	2615	−0.01	1.02	1.02	[11]
5	A470 steel (in)	–	−86.5	2384	0.01	0.95	0.98	[12]
6	2CrNiMoV steel (in)	565	−82.5	2196	−0.07	1.16	1.13	[13]
7	NVA (in)	218	−72.1	1783	−0.01	1.05	0.99	[11]
8	3CrNiMoV steel (in)	550	−67.4	1695	0.05	0.97	0.94	[14]
9	WF-70 weld (in)	740	−63.5	1521	0.01	1.01	0.99	[15]
10	HSST weld 73W (in)	513	−61.3	1472	−0.01	0.95	1.00	[16]
11	HSST weld 72W (in)	496	−60.4	1455	−0.02	0.97	1.00	[16]
12	A533 steel JRQ (in)	480	−59.7	1433	−0.01	1.06	1.06	[17]
13	WF-70 weld (in)	790	−55.8	1330	0	0.96	0.99	[15]
14	A508 steel (TSE-5&6)	605	−52.2	1242	−0.13	1.19	1.20	[18]
15	KWO RPV	–	−49.2	1205	0.04	0.93	0.95	[19]
16	A508 steel	–	−48.0	1175	0.02	0.94	0.98	[12]
17	A508 steel (TSE-7)	450	−32.7	880	−0.10	1.22	1.17	[18]
18	A533 steel	–	−28.5	786	−0.01	1.11	1.01	[12]
19	A508 steel (TSE-5&6)	710	−20.1	723	−0.02	1.40	1.02	[18]
20	NiCrMoV steel	925	−11.3	685	−0.08	2.09	2.20	[11]
21	E36	303	21.2	357	0.04	1.22	0.82	[11]
22	WF-70 weld (irr)	930	24.9	345	0.03	1.11	1.05	[15]
23	HSST weld 72W (irr)	620	29.3	333	−0.07	2.23	1.06	[16]
24	HSST weld 73W (irr)	648	37.2	291	−0.04	0.97	1.03	[16]
25	A533B steel	–	39.9	259	−0.20	1.38	1.27	[20]

Continued Table 1

1	2	3	4	5	6	7	8	9
26	2.5CrMoV steel (embr)	730	45.6	241	0	1.28	1.12	[3]
27	WF-70 weld (irr)	860	49.0	211	−0.08	1.28	1.10	[15]
28	2CrNiMoV steel (embr)	900	57.1	199	−0.65	4.72	2.50	[21]
29	NP2	676	69.0	161	−0.23	2.31	2.26	[11]
30	A533 steel JRQ (irr)	630	86.9	142	−0.01	1.34	0.92	[17]
31	Weld KS01 (irr)	820	137	73.4	−0.38	5.05	2.28	[22]
32	2.5CrMoV steel PTS-1 (embr)	1037	164	65.9	−0.18	14.87	4.37	[23]
33	Weld KS01 (irr)	950	251	21.5	−0.22	3.28	2.30	[18]
34	3CrNiMo steel (irr)	931	130.6	79	−0.62	2.34	1.92	[4]
35	A508 steel (embr)	–	66	164	−0.16	3.54	3.03	[24]

Note. Here and in Table 2: in the bracket the condition of a material is designated as follows: in – received (initial) condition, embr – thermally embrittled condition, irr – irradiated condition.

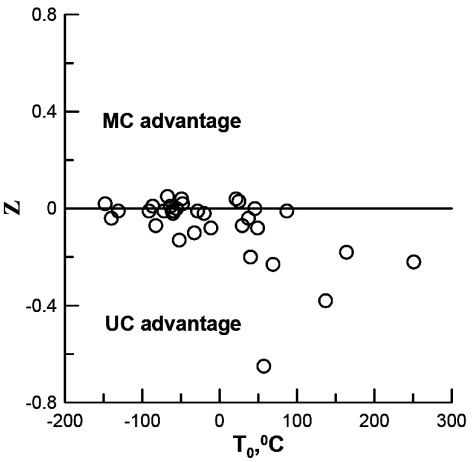

Fig. 4. Comparison of the MC and UC with the parameters Z calculated with Eq. (7) for the data sets described in Table 1.

Thus, it may be concluded that all three statistical parameters provide the same results, at least, for the considered data sets. It means that the reason of the contradictory conclusions in [3, 4] and in [6] cannot be connected with one or another statistical parameter used for comparison.

It should be noted that in [6] two data sets – 28 and 34 sets from Table 1 were also treated with the L parameter. These sets were obtained by the authors of the present paper and published in [21] (set 28) and in [4] (set 34).

However there are significant disagreement between the numerical values of the parameter Z [see Eq. (7)] for sets 28 and 34 as given in [6] and in Table 1. For set 28 according to [6] $Z = -0.03$ and according to Table 1 $Z = -0.65$. For set 34 according to [6] $Z = -0.08$ and according to Table 1 $Z = -0.62$. These different values of Z result in quite different conclusions in [6] and here. The calculation results in Table 1 show that the UC has advantage as compared with the MC for these data sets. According to [6] the UC

and MC methods give practically the same predictions. We could not find out the reason of such disagreement in numerical values of the parameter Z. It may be supposed only that for analysis in [6] these data sets were additionally somehow treated, and at the same time the values of Z for sets 28 and 34 given in Table 1 were calculated allowing for all experimental points.

One more possible reason of contradictory conclusions in [3, 4] and in [6] may consist in the using of different K_{JC} data sets. In [6] 50 large data sets were considered that include experimental K_{JC} values for compact tension (CT) specimens and for single-edge bending (SEB) specimens, in particular, for pre-cracked Charpy (PCC) specimens.

To expand the data base, in addition to 35 large data sets in [3, 4] (see Table 1), we analyze here some more data sets from ones in [6]. These additional data sets have been taken on the following requirements.

1. *First of all, these data have to be obtained by CT specimens testing, i.e., fracture toughness data for PCC (SE(B)-10 mm) specimens should not be used*.

This requirement is explained by the known particularities of fracture toughness data for PCC specimens. It is known [25–27] that K_{JC} values obtained by testing PCC specimens have larger scatter than CT specimens and large number of incorrect values, moreover the test temperature range when K_{JC} values are correct is significantly narrow than for CT specimens with thickness $B \geq 12.5$ mm.

As a rule, K_{JC} values from PCC specimens are larger than K_{JC} values from CT specimens that expresses in a difference of T_0 values for these specimens [27]. When temperature increases a difference in K_{JC} values for PCC and CT specimens increases [25, 26]. As a result, the $K_{JC}(T)$ curve for PCC specimens is steeper than the curve for CT specimens.

Detailed study of the particularities of fracture toughness data for PCC and CT specimens was performed in [25, 26]. The ratio $J_{PCC}/J_{CT-0.5}$ as a function of the parameter $M = b\sigma_Y/J_{PCC}$ was obtained in [26] and shown in Fig. 5. Here J_{PCC} and $J_{CT-0.5}$ are J-integral values for PCC and CT-0.5 specimens, respectively, σ_Y is the yield stress, and b is the reminding ligament.

It is seen from Fig. 5 that when the parameter M decreases, i.e., the value J_{PCC} increases the ratio $J_{PCC}/J_{CT-0.5}$ increases. Applying these data for the $J_{PCC}(T)$ and $J_{CT-0.5}(T)$ curves and taking into account that the J_{PCC} values increase with temperature increasing the conclusion may be drawn that the $J_{PCC}(T)$ curve is steeper than the $J_{CT-0.5}(T)$ curve.

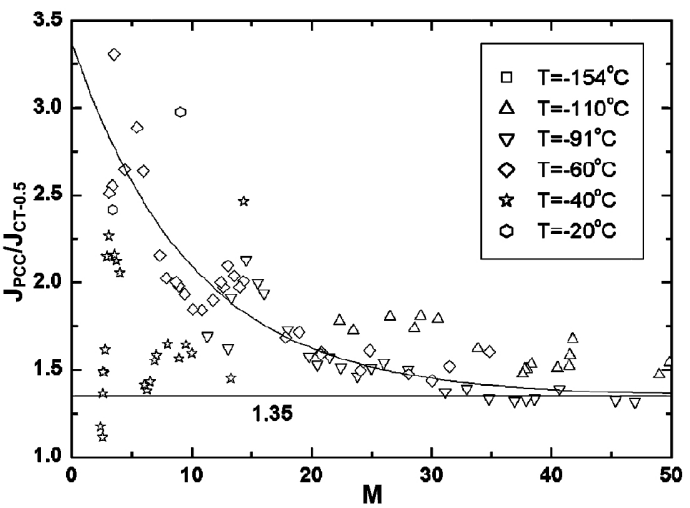

Fig. 5. The ratio $J_{PCC}/J_{CT-0.5}$ vs the parameter M according to [26].

On the basis of the performed studies the authors of paper [25] concluded: "The differences in fracture toughness between standardized CT specimens and pre-cracked Charpy specimens can not be verified in the conventional way by using statistical weakest link size effect predictions and specimen size criteria as proposed in test standards."

One more example of steeper $K_{JC}(T)$ curve for PCC specimens as compared with the $K_{JC}(T)$ curve for CT-2T specimens is shown in Fig. 6. $K_{JC}(T)$ curves here have been constructed for 2CrNiMoV steel (set 6 in Table 1) by the following way. Firstly, the values of $K_{JC(med)j}$ have been determined for each test temperature. Then the obtained $K_{JC(med)j}$ values have been approximated by a function $K_{JC} = a + b\exp(cT)$. The difference in the shapes for the obtained curves is seen in Fig. 6.

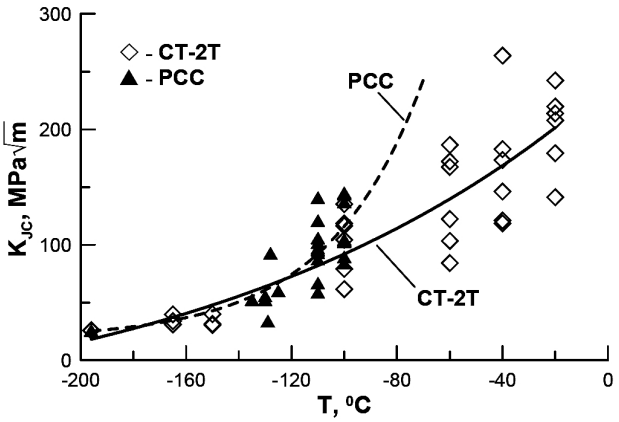

Fig. 6. The $K_{JC}(T)$ curves obtained by treatment of the fracture toughness data for CT-2T and PCC specimens with equation $K_{JC} = a + b\exp(cT)$ for 2CrNiMoV steel in initial condition: the test results for CT-2T specimens [13] correspond to set 6 in Table 1 and the test results for PCC were used previously in [28, 29]. (All the data have been recalculated for 25 mm.)

The above reasons show that it is not reasonable to use K_{JC} values from PCC specimens for objective comparison of the MC and UC methods as the main difference between these methods consists exactly in the description of the $K_{JC}(T)$ curve shape. As the steepness of $K_{JC}(T)$ curves obtained from the test results of PCC specimens is overestimated as compared with KJC(T) curves from CT specimens the MC will describe K_{JC} values for PCC specimens better than the UC. This is clear seen from Fig. 2 where the comparison results for PCC and CT specimens are shown as represented in [6].

2. *The second requirement is that the number of incorrect results in data set should be sufficiently small*.

This requirement is connected with the following reasons.

Incorrect experimental results damage the standard distribution on K_{JC} both for case of censoring of incorrect experimental data and for case when incorrect experimental data are considered as correct ones. If incorrect experimental data (due to exceeding of K_{JC} capacity, $K_{JC(lim)}$ [1]) are considered as correct ones then the scatter of K_{JC} increases as compared with the scatter for standard K_{JC} distribution, and K_0 is overestimated. If incorrect experimental data are censored then K_0 may be both underestimated and overestimated.

For most cases of incorrect results *J*-integral does not control the stress-and-strain fields near a crack tip. It is clear if we want to determine which $K_{JC}(T)$ curve – predicted with the MC or with the UC curve is closer to real $K_{JC}(T)$ curve we should use such K_{JC} values for that *J*-integral controls stress-and-strain fields near the crack tip, i.e., $K_{JC} < K_{JC(lim)}$.

Therefore, the database containing, for the most part, correct experimental data should be taken for objective comparison of the MC and UC methods.

Some data sets used in [6] contain large number of incorrect experimental data that results in the necessity to use the censoring procedure. For example, the data used in [6] and represented in [30] contain more than 30% incorrect results, and this number increases with temperature increase.

3. *The third requirement is that the experimental* K_{JC} *values for a chosen set should be obtained over wide range of test temperatures*.

This requirement is quite clear as it is well known that when K_{JC} values are obtained over narrow temperature range they may be fitted by any function practically with small error.

Thus, in addition to 35 data sets in Table 1 we succeed in finding and in analyzing here 9 data sets from ones in [6] that satisfy the above requirements. These additional data sets and the results of their treatment with the MC and UC are represented in Table 2. (The data sets from Table 1 are also included once more in Table 2 as they are needed for further analysis.)

It should be mentioned that unfortunately, a series of the data sets considered in [6] could not be analyzed and estimations made in [6] could not be commented. For example, in [34] two data sets were represented with approximately 400 test results in each sets, and in [6] only 18 correct results were selected from these data sets. It is difficult to determine which results were taken and what requirement for selection was used in [6].

We tried to include in Table 2 the most interesting sets (from viewpoint of the MC and UC comparison). These sets are sets with the maximum difference between the values $\ln L^{MC}/r$ and $\ln L^{UC}/r$ for benefit of the MC according to [6].

The maximum value of the parameter Z calculated by Eq. (7) is equal to 0.91 [6] for the data set for A470 steel represented in [31]. For this set the parameter T_0 is equal to 86°C as calculated in [6].

Unfortunately, we could not analyze this data set as we failed to find it. Begley and Toolin [31] represent two K_{JC} data sets for two materials denoted as FD 1196 and HD 9980 of one steel grade (NiCrMoV). These data sets were obtained by testing CT specimens with thicknesses from 50 to 200 mm. These sets are included in Table 2 as sets 36 and 37.

The calculations performed provide for FD 1196 material (set 36 in Table 2) $T_0 = -12.7$°C and $Z = 0.2$, and for HD 9980 (set 37 in Table 2) $T_0 = -7$°C and $Z = 0.32$. It is seen that these estimations significantly differ from those in [6]. Probably, the wrong reference ([31]) was given in [6] for A470 steel.

Nevertheless, the data sets for FD 1196 and HD 9980 materials taken from [31] appear to be very useful. These data (sets 36 and 37 in Table 2) allow us to reveal very important issue when determining the $K_{JC}(T)$ curve shape.

The obtained values of the parameter Z (see Table 2) show some preference for the MC for FD 1196 and HD 9980 materials. The question arises whether it is connected with the $K_{JC}(T)$ curve shape or with another reason.

The analysis of the data sets for FD 1196 and HD 9980 materials and the results of their treatment with the MC and UC have shown that the difference between $\ln L^{MC}/r$ and $\ln L^{UC}/r$ is caused mainly by the difference in the low shelf, K_{JC}^{shelf}, values. The fact of the matter is that when calculating the parameter L the K_{JC} values obtained near the low shelf of $K_{JC}(T)$ curve have very large weight as compared with the K_{JC} values at higher temperatures. At the same time it is clear that the low shelf value does not practically affect the $K_{JC}(T)$ curve shape.

Table 2

The Results of Treatment of the Extended Data Base with Three Statistical Parameters (L, δ, and σ) for Different and Equal K_{JC}^{shelf} Values for the UC and MC

No.	Material	σ_Y at $T = 20$°C, MPa	T_0, °C	UC: $K_{JC}^{shelf} = 26$ MPa$\sqrt{\text{m}}$, MC: $K_{JC}^{shelf} = 30$ MPa$\sqrt{\text{m}}$				UC and MC $K_{JC}^{shelf} = 30$ MPa$\sqrt{\text{m}}$				Reference
				Ω, MPa$\sqrt{\text{m}}$	Z	$\frac{\delta_{MC}}{\delta_{UC}}$	$\frac{\sigma_{MC}}{\sigma_{UC}}$	Ω, MPa$\sqrt{\text{m}}$	Z	$\frac{\delta_{MC}}{\delta_{UC}}$	$\frac{\sigma_{MC}}{\sigma_{UC}}$	
1	2	3	4	5	6	7	8	9	10	11	12	13
1	A533B steel (in)	567	−148.0	7397	0.02	0.91	1.06	7132	0	1.02	1.01	[11]
2	A508 steel (in)	650	−140.0	6441	−0.04	0.91	0.94	6180	−0.01	1.04	1.03	[11]
3	HY130L (in)	955	−131.0	5405	−0.01	0.92	0.98	5128	−0.01	1.01	1.01	[11]
4	ABS DS (in)	270	−91.3	2615	−0.01	1.02	1.02	2419	−0.07	1.11	1.12	[11]
5	A470 steel (in)	–	−86.5	2384	0.01	0.95	0.98	2249	−0.01	1.05	1.01	[12]
6	2CrNiMoV steel (in)	565	−82.5	2196	−0.07	1.16	1.13	2062	−0.08	1.31	1.27	[13]
7	NVA (in)	218	−72.1	1783	−0.01	1.05	0.99	1752	0.02	1.03	0.99	[11]
8	3CrNiMoV steel (in)	550	−67.4	1695	0.05	0.97	0.94	1561	−0.03	1.32	1.1	[14]
9	WF-70 weld (in)	740	−63.5	1521	0.01	1.01	0.99	1483	0.04	0.89	0.98	[15]
10	HSST weld 73W (in)	513	−61.3	1472	−0.01	0.95	1.0	1413	0	0.96	0.98	[16]
11	HSST weld 72W (in)	496	−60.4	1455	−0.02	0.97	1.0	1397	−0.02	0.99	1.02	[16]
12	A533 steel JRQ (in)	480	−59.7	1433	−0.01	1.06	1.06	1357	−0.05	1.16	1.13	[17]
13	WF-70 weld (in)	790	−55.8	1330	0	0.96	0.99	1256	−0.02	1.04	1.01	[15]
14	A508 steel (TSE-5&6)	605	−52.2	1242	−0.13	1.19	1.2	1205	−0.15	1.25	1.25	[18]
15	KWO RPV	–	−49.2	1205	0.04	0.93	0.95	1098	−0.02	1.04	1.03	[19]
16	A508 steel	–	−48.0	1175	0.02	0.94	0.98	1088	−0.01	1.1	1.07	[12]
17	A508 steel (TSE-7)	450	−32.7	880	−0.10	1.22	1.17	842	−0.10	1.3	1.23	[18]
18	A533 steel	–	−28.5	786	−0.01	1.11	1.01	746	0	1.53	0.99	[12]
19	A508 steel (TSE-5&6)	710	−20.1	723	−0.02	1.40	1.02	653	−0.15	1.23	1.2	[18]
20	NiCrMoV steel	925	−11.3	685	−0.08	2.09	2.2	584	−0.50	2.86	3.05	[11]
21	E36	303	21.2	357	0.04	1.22	0.82	306	−0.18	1.6	1.61	[11]

Continued Table 2

1	2	3	4	5	6	7	8	9	10	11	12	13
22	WF-70 weld (irr)	930	24.9	345	0.03	1.11	1.05	324	−0.03	1.21	1.07	[15]
23	HSST weld 72W (irr)	620	29.3	333	−0.07	2.23	1.06	323	−0.07	2.11	1.07	[16]
24	HSST weld 73W (irr)	648	37.2	291	−0.04	0.97	1.03	278	−0.07	0.96	1.03	[16]
25	A533B steel	–	39.9	259	−0.20	1.38	1.27	220	−0.47	1.82	1.62	[20]
26	2.5CrMoV steel (embr)	730	45.6	241	0	1.28	1.12	202	−0.18	1.91	1.47	[3]
27	WF-70 weld (irr)	860	49.0	211	−0.08	1.28	1.10	197	−0.11	1.5	1.14	[15]
28	2CrNiMoV steel (embr)	900	57.1	199	−0.65	4.72	2.5	185	−0.71	6.63	2.69	[21]
29	NP2	676	69.0	161	−0.23	2.31	2.26	136	−0.54	3.29	2.98	[11]
30	A533 steel JRQ (irr)	630	86.9	142	−0.01	1.34	0.92	137	0	1.3	0.9	[17]
31	Weld KS01 (irr)	820	137.0	73.4	−0.38	5.05	2.28	70	−0.37	4.93	2.24	[22]
32	2.5CrMoV steel PTS-1 (embr)	1037	164.0	65.9	−0.18	14.87	4.37	63	−0.10	13.4	4.29	[23]
33	Weld KS01 (irr)	950	251.0	21.5	−0.22	3.28	2.3	19.2	0.11	3.05	2.16	[18]
34	3CrNiMo steel (irr)	931	130.6	79	−0.62	2.34	1.92	73	−0.64	2.4	1.87	[4]
35	A508 steel (embr)	–	66.0	164	−0.16	3.54	3.03	155	−0.15	3.7	3.05	[24]
36	NiCrMoV steel (FD 1196)	910	−12.7	682	0.20	0.94	0.90	588	−0.14	1.62	1.31	[31]
37	NiCrMoV steel (HD 9980)	1050	−7.4	737	0.32	0.84	0.81	514	−0.50	1.69	1.83	[31]
38	A533B weld	600	111.7	80	−0.13	0.60	0.82	73	0.17	0.53	0.76	[32]
39	A533B C1.1	600	73.3	148	−0.17	2.49	1.29	132	−0.23	4.23	1.36	[32]
40	A533B weld	600	19.5	356	−0.06	0.97	1.01	326	0.08	0.82	0.88	[32]
41	CrMoV steel	620	62.0	206	0.39	0.63	0.60	147	−0.12	1.32	1.06	[33]
42	CrMoV steel	640	47.0	223	−0.06	1.16	1.22	193	−0.08	1.66	1.45	[33]
43	NiMoV steel	570	22.2	382	−0.01	0.74	0.76	294	−0.04	1.13	1.07	[33]
44	17MoV84 steel	1082	180	63	−0.70	8.48	5.20	60	−0.58	8.11	5.07	[6]

As seen from Eqs. (8) and (9), for the UC $K_{JC}^{shelf} = 26\ \text{MPa}\sqrt{\text{m}}$ and for the MC $K_{JC}^{shelf} = 30\ \text{MPa}\sqrt{\text{m}}$. The difference in K_{JC}^{shelf} that is equal to 4 $\text{MPa}\sqrt{\text{m}}$ may result in the difference between $\ln L^{MC}/r$ and $\ln L^{UC}/r$. For HD 9980 material one K_{JC} value near the low shelf is equal to 48 $\text{MPa}\sqrt{\text{m}}$ [31] for CT specimen with the thickness of 50 mm that is clearly overestimated.

This overestimated K_{JC} value results in the revealed preference for the MC as compared with the UC. If the K_{JC}^{shelf} value is taken the same for the MC and UC, for example, $K_{JC}^{shelf} = 30\ \text{MPa}\sqrt{\text{m}}$ then we obtain for FD 1196 material $Z = -0.14$, and for HD 9980 $Z = -0.5$ (see Table 2). It means than the UC better describes the $K_{JC}(T)$ curve shape than the MC.

This example has shown that when using the maximum likelihood method (the parameter L) a seeming advantage of one method over another may be caused by a difference in the K_{JC}^{shelf} values but not a difference in the shape for the experimental and predicted $K_{JC}(T)$ curves. This is a result of a large contribution of K_{JC} values near the low shelf in the parameter L and a weak influence of these values on the $K_{JC}(T)$ curve shape.

Thus, as a common case, the comparison of the MC and UC methods with the test results is advisable to make for the same K_{JC}^{shelf} level.

The results of treatment of all the data sets with three parameters L, δ, and σ are represented in Table 2 and in Figs. 7–9. Table 2 includes the sets 1–35 used earlier in [3, 4] and additional sets 36–44 taken from the references given in [6].

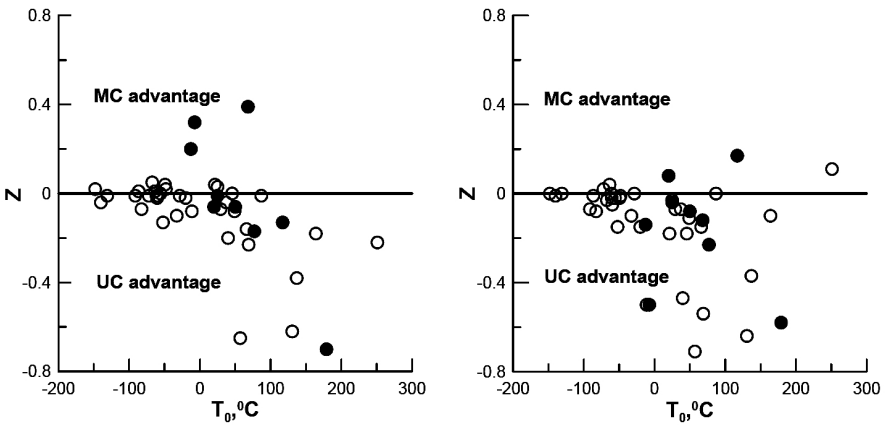

Fig. 7. Comparison of the MC and UC with the parameters Z calculated with Eq. (7) for the data sets described in Table 2. [Here and in Figs. 8 and 9: open symbols – sets 1–35, closed symbols – sets 36–44: (a) calculations for different K_{JC}^{shelf} values: $K_{JC}^{shelf} = 26\ \text{MPa}\sqrt{\text{m}}$ for the UC and $K_{JC}^{shelf} =$ $= 30\ \text{MPa}\sqrt{\text{m}}$ for the MC; (b) calculations for the same K_{JC}^{shelf} value taken as $K_{JC}^{shelf} = 30\ \text{MPa}\sqrt{\text{m}}$.]

Treatment was performed for two variants. The first variant is the comparison for different K_{JC}^{shelf} values: $K_{JC}^{shelf} = 26\ \text{MPa}\sqrt{\text{m}}$ for the UC and $K_{JC}^{shelf} = 30\ \text{MPa}\sqrt{\text{m}}$ for the MC. For the second variant the same K_{JC}^{shelf} value was taken as $K_{JC}^{shelf} = 30\ \text{MPa}\sqrt{\text{m}}$.

The results represented in Table 2 and in Figs. 7–9 allow one to reveal the following findings.

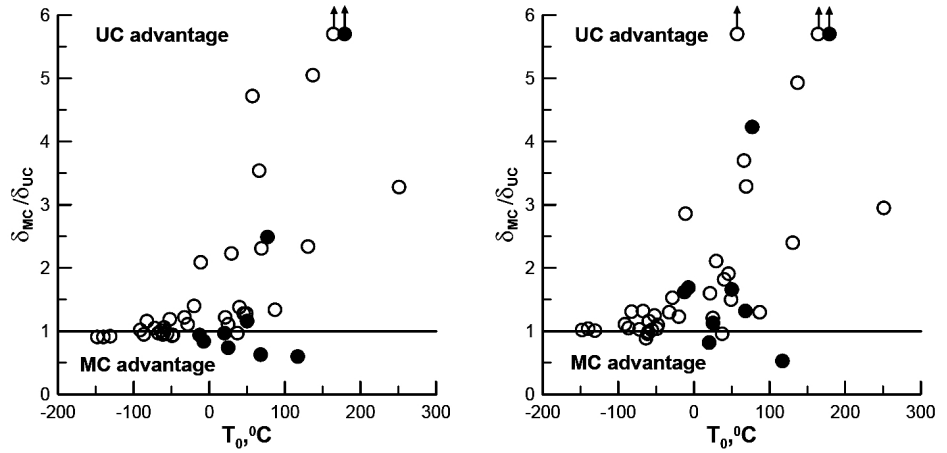

Fig. 8. Comparison of the MC and UC with the parameters δ calculated with Eq. (1) for the data sets described in Table 2.

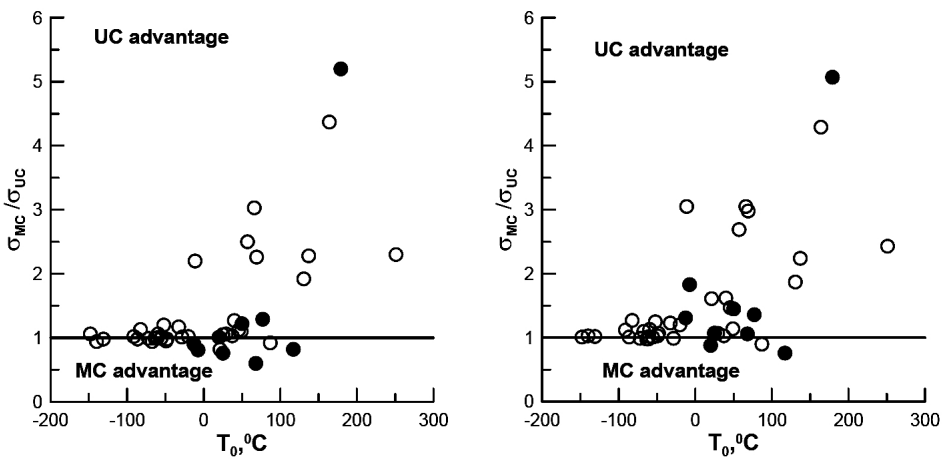

Fig. 9. Comparison of the MC and UC with the parameter σ calculated with Eq. (4) for the data sets described in Table 2.

1. All three parameters L, δ, and σ provide similar results when comparing the MC and UC.

2. Conclusion made in [3, 4] on the basis of 35 data sets is confirmed for the extended data sets including 9 sets from [6]. This conclusion is that for materials in the initial (as-received) condition and with small degrees of embrittlement (when the T_0 value is low) the curves predicted with both methods coincide practically, and when the degree of embrittlement increases (i.e., T_0 increases), the description of $K_{JC}(T)$ with the Unified Curve becomes more adequate than with the MC as the UC takes into account change in the $K_{JC}(T)$ curve shape.

3. When using the maximum likelihood method, i.e., the parameter L, the comparison of the MC and UC methods with the test results is advisable to make for the same K_{JC}^{shelf} level. For this case as it is seen from Fig. 7b the above conclusion becomes even more evident.

3. **Discussion**. The performed comparison has shown once more that the experimental $K_{JC}(T)$ curves for ferritic steels may be adequately described both with the MC and UC methods when degree of embrittlement is not high, i.e., the T_0 value is low. When the degree of embrittlement increases (i.e., T_0 increases), the description of $K_{JC}(T)$ with the Unified Curve becomes more adequate than with the MC as the experimental $K_{JC}(T)$ curves change their shape.

Additionally, it is of interest to note that both methods allow the description of $K_{JC}(T)$ curves for various ferritic steel for which the yield stress σ_Y varies over wide range, from $\sigma_Y \approx 200$ MPa to $\sigma_Y \approx 1100$ MPa.

So, several principal questions arise here as follows:

(i) why the $K_{JC}(T)$ dependences for quite different ferritic steels may be described by the same function taken as the MC or UC;

(ii) why the $K_{JC}(T)$ curves obey the lateral temperature shift condition when degree of embrittlement is not high;

(iii) why the $K_{JC}(T)$ curves change their shape when degree of embrittlement increases significantly.

In the present section an attempt is undertaken to answer these questions and to find some physical background for the above properties.

These issues may be considered on the basis of local brittle fracture criteria. The analysis hereafter is based on local criterion of cleavage fracture formulated and verified in [35–40]. This criterion allows not only the prediction of the $K_{JC}(T)$ curves for RPV materials [13, 14, 21, 38, 39] but also the analysis of other brittle fracture properties for RPV steels such as the WPS effect [41], the plastic tearing effect [42], the biaxial loading effect [43].

This local criterion is written in the form

$$\sigma_{nuc} \equiv \sigma_1 + m_{T\varepsilon}\sigma_{eff} \geq \sigma_d\,, \tag{13a}$$

$$\sigma_1 \geq S_C(\kappa), \tag{13b}$$

where σ_1 is the maximum principal stress, σ_{eff} is the effective stress, $\sigma_{eff} = \sigma_{eq} - \sigma_Y$, σ_{eq} is the equivalent stress, σ_Y is the yield stress, σ_d is the critical stress for microcrack nucleation, $m_{T\varepsilon}$ is the concentration coefficient for the local stress near the microcrack-nucleating particles, S_C is the critical brittle fracture stress, which is generally assumed to be independent of temperature, strain rate, and stress triaxiality, κ is the accumulated plastic strain, $\kappa = \int d\varepsilon^p_{eq}$, and $d\varepsilon^p_{eq}$ is the equivalent plastic strain increment. The coefficient $m_{T\varepsilon}$ depends on temperature T and plastic strain.

From the physical viewpoint, the first condition is the condition for the nucleation of cleavage microcracks, and the second one – the condition of their propagation. The parameter σ_d is the strength of carbides or carbide-matrix interfaces or other particles on which cleavage microcracks are nucleated. This parameter depends on degree of material embrittlement and does not depend on temperature, strain rate and stress triaxiality. The parameter σ_d has been linked with neutron fluence on the basis of the developed models of the influence of the radiation defects on cleavage microcrack nucleation [44]. The parameter S_C is interpreted as the stress required for Griffith's crack start and propagation through various barriers (grain boundaries, microstresses, slip bands, boundaries of dislocation substructure).

The functions $S_C(\kappa)$ and $m_{T\varepsilon}(T, \kappa)$ are calculated as [35–40]

$$S_C(\kappa) = [C_1 + C_2 \exp(-A_d\kappa)]^{-1/2}, \tag{14}$$

$$m_{T\varepsilon}(T, \kappa) = m_T(T) m_\varepsilon(\kappa), \tag{15}$$

$$m_\varepsilon(\kappa) = S_0 / S_C(\kappa), \tag{16}$$

$$m_T(T) = m_0 \sigma_{Ys}(T), \tag{17}$$

where C_1, C_2, and A_d are material constants, $S_0 \equiv S_C(\kappa = 0)$ is the stress of start for the nucleus microcrack, m_0 is a constant which may be experimentally determined, and σ_{Ys} is the temperature-dependent component of the yield stress.

The dependence $\sigma_Y(T)$ should be given by equation [45]

$$\sigma_Y(T) = \sigma_{YG} + \sigma_{Ys}(T), \tag{18}$$

where σ_{YG} is the temperature-independent (athermal) component of the yield stress.

According to criterion (13) the brittle fracture on a macro-scale may be controlled by both microcrack nucleation (13a) and microcrack propagation conditions (13b) that depends on material properties and loading conditions, mainly, on stress triaxiality and temperature [44].

Prediction of brittle fracture on a macroscale on the basis of criterion (13) may be performed in a deterministic manner [35, 36] and in a stochastic manner with the Prometey model [21, 38, 40]. The Prometey model uses the Weibull statistics for stochastic parameters σ_d and S_C and the weakest link model to predict the brittle fracture on a macroscale. The Prometey model was verified by application to RPV steels in various conditions (initial, irradiated, and highly embrittled) [21, 38]. It has been shown [44] that the Prometey model provides not only a prediction of the $K_{JC}(T)$ curve allowing for possible variation in the $K_{JC}(T)$ curve shape but also a prediction of lateral shift of $K_{JC}(T)$ curves. The Unified Curve method was proposed just on the basis of the Prometey model [3]. The Unified Curve method as well as the Prometey model predicts a possible variation in $K_{JC}(T)$ curve shape under irradiation.

Criterion (13) and the Prometey model allow the explanation of the main properties of the $K_{JC}(T)$ curve and its transformation under irradiation. For explanation it should be have in mind that the parameters σ_d and S_C do not depend on temperature and the parameter $\sigma_{eff} = \sigma_{eq} - \sigma_Y$ is weakly sensitive to temperature as it characterizes the strain hardening. Then it follows from Eqs. (13)–(17) that the temperature dependence of fracture toughness is mainly controlled by the temperature dependence of the yield stress, $\sigma_Y(T)$, more exactly, by the dependence $\sigma_{Ys}(T)$.

When degree of embrittlement increases the parameter σ_d decreases and for most cases the parameter S_C does not vary*. According to the Prometey model the transformation of $K_{JC}(T)$ curve is caused by the following reasons: (i) decrease in σ_d, (ii) increase in σ_Y, and (iii) variation of the contributions of two terms in $\sigma_{nuc} \equiv \sigma_1 + m_{T\varepsilon}\sigma_{eff}$ [see Eq. (13a)]. These contributions depend on temperature.

According to the Prometey model it is worthwhile to consider three temperature ranges *I*, *II*, and *III* as shown in Fig. 10. When the variation of K_{JC} from the lower up to upper shelves occurs over low temperature range *I* (that corresponds to low T_0 values) the second term in $\sigma_{nuc} \equiv \sigma_1 + m_{T\varepsilon}\sigma_{eff}$ is significantly larger than the first term ($\sigma_1 << m_{T\varepsilon}\sigma_{eff} \approx m_0 \sigma_{Ys}\sigma_{eff}$) as the concentration coefficient $m_{T\varepsilon}$ of the effective stress is very large due to large value of $\sigma_{Ys}(T)$. For this case according to the Prometey model the transformation of the $K_{JC}(T)$ curve caused by decrease in σ_d and increase in σ_Y obeys the lateral temperature shift condition (see Fig. 10).

* Significant segregation of impurities on grain boundaries, for example, under temper embrittlement of material with high content of phosphorus, may result in decreasing S_C.

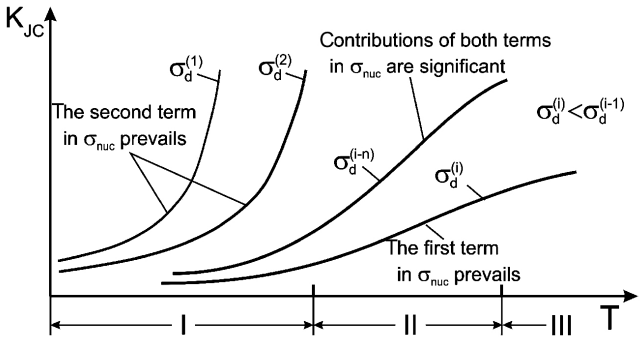

Fig. 10. Transformation of $K_{JC}(T)$ curve for the irradiated materials according to the Prometey model and criterion (13).

As temperature increases the first term in σ_{nuc} becomes comparable with the second term so that over temperature range *II* the contributions of both terms are significant.

Over temperature range *III* the value of $\sigma_{Ys}(T)$ is small and, as a result, $m_T(T)$ is also small and the first term (σ_1) in σ_{nuc} prevails.

According to the Prometey model for temperature ranges *II* and *III* the lateral temperature shift condition is not valid and the shape of $K_{JC}(T)$ curve varies as degree of material embrittlement increases (see Fig. 10).

For all the temperature ranges (*I*, *II*, and *III*) the $K_{JC}(T)$ curve shape is controlled by the dependence $\sigma_{Ys}(T)$, however a link of the $K_{JC}(T)$ curve shape and the dependence $\sigma_{Ys}(T)$ is different for each temperature range.

The temperature dependence $\sigma_{Ys}(T)$ may be approximated by equation [38]

$$\sigma_{Ys}(T) = b\exp(-h(T+273)), \tag{19}$$

where b and h are the material constants independent of temperature, and T is the temperature in °C.

The test results show that different ferritic steels have practically the same dependence $\sigma_{Ys}(T)$ although they have different dependencies $\sigma_Y(T)$. Figure 11 demonstrates the temperature dependencies $\sigma_{Ys}(T) = \sigma_Y(T) - \sigma_{YG}$ for various ferritic steels. The list of materials represented in Fig. 11 is given in Table 3.

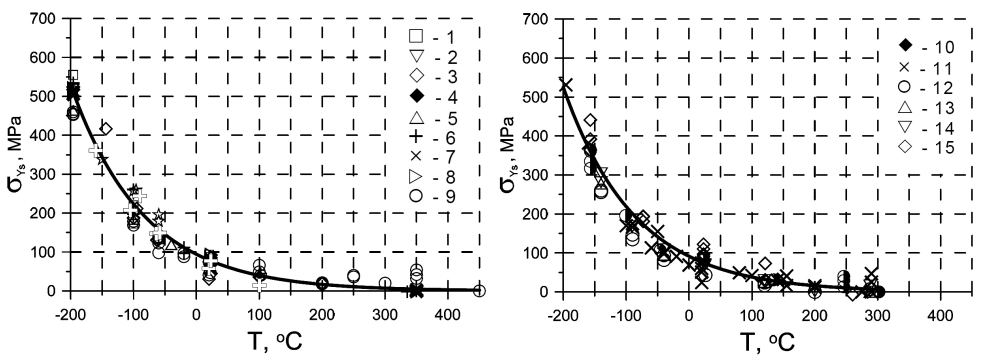

Fig. 11. The temperature dependence of the thermal part $\sigma_{Ys}(T)$ of the yield stress for the materials detailed in Table 3 (the numbers in figures correspond to those in Table 3): symbols are experimental data for Russian WWER steels and its welds (a) and for A533 steels and its welds (b); curve is their approximation with Eq. (20).

T a b l e 3

The List of Materials Represented in Fig. 11

No.	Material	Condition	σ_Y at $T = 20$°C, MPa	σ_{YG}, MPa
Original experimental data				
1	1.5Mn–0.7Si steel (modified)	initial	309	267
2	2.2Mn–0.7Si weld	ditto	357	290
3	1.5Mn–0.7Si steel	ditto	365	307
4	1.5Mn–0.7Si steel (modified)	irradiated, $F = 1 \cdot 10^{19}$ cm^{-2}	500	431
5	Mn–2Ni–Mo–V steel	initial	525	456
6	2Cr–Ni–Mo–V steel	ditto	580	510
7	2Cr–Ni–Mo–V steel	irradiated, $F = 2.5 \cdot 10^{19}$ cm^{-2}	638	569
8	3Cr–Mo–V weld	irradiated, $F = 2.5 \cdot 10^{19}$ cm^{-2}	639	556
9	2Cr–Ni–Mo–V steel	thermal embrittled	900	846
Available experimental data [46–48]				
10	A533-B steel	initial	461	379
11	JRQ steel	ditto	467	415
12	A533 gr.B cl.1 (HSST Plate 02)	ditto	487	424
13	Weld 68 (HSST Plate 02)	ditto	–	494
14	Weld 69 (HSST Plate 02)	ditto	638	569
15	A533-B steel	irradiated, $F = (1.7–2.4) \cdot 10^{19}$ cm^{-2}	668	565

The experimental data obtained by the authors of the present study are shown in Fig. 11a, and the results taken from [46–48] are represented in Fig. 11b. It is clearly seen from Fig. 11 that all the experimental data are sufficiently well approximated by the same curve. Only one exception may be observed in Fig. 11a. These data are the points located over the temperature range of 250–350°C for 2CrNiMoV steel in thermal embrittled condition. This result is explained by dynamic thermal aging processes under tensile testing. Outside of the indicated temperature range the experimental values of σ_{Ys} correspond to the common curve.

Treatment of all experimental results on $\sigma_{Ys}(T)$ (excepting experimental data for 2CrNiMoV steel in thermal embrittled condition over the temperature range of 250–350°C) by Eq. (19) gives: $b = 993$ MPa and $h = 8.74 \cdot 10^{-3}$ °C^{-1}. As a result, for the considered ferritic steels

$$\sigma_{Ys}(T) = 993 \exp(-8.74 \cdot 10^{-3} (T + 273)). \quad (20)$$

According to the Prometey model over low temperature range the transformation of $K_{JC}(T)$ curve is described by the lateral temperature shift, by other words, the $K_{JC}(T)$ curve shape does not vary.

Thus, over low temperature range (low values of T_0) the following properties have been found: (i) the $K_{JC}(T)$ curve shape does not vary; (ii) the $K_{JC}(T)$ curve shape is controlled by the $\sigma_{Ys}(T)$ dependence; and (iii) the dependencies $\sigma_{Ys}(T)$ for different ferritic steels may be approximated by the same function.

These properties explain why for low values of T_0 the $K_{JC}(T)$ curves for quite different ferritic steels may be described by the same function. (It does not matter what function – MC or UC is used.) For this case the very simple correlation may be found between the function describing $K_{JC}(T)$ [see Eq. (8)] and the function describing $\sigma_{Ys}(T)$ [see Eqs. (19) and (20)]

$$\gamma \approx 2h. \tag{21}$$

According to the Prometey model the shape of $K_{JC}(T)$ curve varies as degree of material embrittlement increases (see Fig. 10). This result is mainly connected with an increasing contribution of σ_1 in σ_{nuc} [see Eq. (13a)].

The effect of σ_1 on $K_{JC}(T)$ curve shape may be understood when considering temperature range *III*. For extremely embrittled materials when $K_{JC}(T)$ curve located in elevated temperature range *III* (see Fig. 10) the value σ_1 mainly contributes to σ_{nuc} [Eq. (13a)] as $\sigma_1 > m_{T\varepsilon}\sigma_{eff} = m_0\sigma_{Ys}\sigma_{eff}\, S_0/S_C$.

The value σ_1 near the crack tip in possible brittle fracture zone is connected with the yield stress σ_Y by relation $\sigma_1 \approx q\sigma_Y$, where the parameter q characterizes the stress triaxiality near the crack tip, $q = \sigma_1/\sigma_{eq}$. Over elevated temperature range the yield stress σ_Y is practically constant therefore the $K_{JC}(T)$ curve shape changes significantly and becomes sloping. Nevertheless, over this temperature range the ratio $\dfrac{1}{\sigma_{Ys}}\dfrac{d\sigma_{Ys}}{dT} \neq 0$ in spite of the fact that $\dfrac{1}{\sigma_Y}\dfrac{d\sigma_Y}{dT} \to 0$. Therefore according to condition (13a) $K_{JC}(T)$ is an increasing function of temperature even when $\sigma_Y(T) \approx$ const, although this curve may be very sloping.

It is appropriate to mention here that according to the widely used stress-controlled local criterion of cleavage fracture it may be shown that $K_{JC}(T) \approx$ const over elevated temperature range. Stress-controlled criterion is traditionally written in the form [49–53]

$$\sigma_{eq} \geq \sigma_Y, \tag{22a}$$

$$\sigma_1 \geq S_C. \tag{22b}$$

In the terms of stress intensity factor, K_J, criterion (22) is written in a deterministic manner as

$$K_{JC} = K_J, \tag{23}$$

when

$$\sigma_1\big|_{r=r_c} = S_C, \tag{24}$$

where r_c is a size of so-called process zone located in the plastic zone near the crack tip.

Thus, it follows from Eqs. (23) and (24) with the account taken of $\sigma_1 \approx q\sigma_Y$ that the temperature dependence of fracture toughness is mainly controlled by the temperature dependence of the yield stress, $\sigma_Y(T)$. As a result, over elevated temperature range *III* according to criterion (22) $K_{JC}(T) \approx$ const. [It should be mentioned that to avoid such situation the brittle fracture models based on criterion (22) introduce a priori an increasing temperature dependence for the parameter S_C (or the parameter σ_u in the terms of the Beremin model).]

Thus the physical processes of cleavage fracture reflected in local criterion (13) allow one to answer the above questions. This analysis has shown that there is physical background to describe $K_{JC}(T)$ curves by the same function for quite different ferritic steels. It is the same dependence $\sigma_{Ys}(T)$ being practically the only temperature-dependent parameter that reflects the thermo-activated nature of brittle fracture.

One more important properties of brittle fracture is not connected directly with local criteria, i.e., with the physical processes, and should be mainly attributed to the basic mechanical features of brittle fracture. This is the relation $P_f \sim K_J^4$ which is used both in the MC and UC methods.

The relation $P_f \sim K_J^4$ follows from the considerations.

1. Plastic deformation is a necessary condition for brittle fracture.

2. Stress and strain fields near the crack tip are self-similar (or by other words, homothetic).

3. Brittle fracture obeys the weakest link concept.

The relation $P_f \sim K_J^4$ is valid for $K_J >> K_{\min}$ and this fact does not depend on the used local criterion of brittle fracture [9, 10]. As a common case, the parameter $K_{\min}$ may be introduced in $P_f(K_J)$ by various ways. Two simplest ways are as follows. The first variant is

$$P_f \sim f(K_J - K_{\min})^4 \qquad \text{for} \qquad K_J > K_{\min}. \tag{25}$$

The second variant is

$$P_f \sim f(K_J^4 - K_{\min}^4) \qquad \text{for} \qquad K_J > K_{\min}. \tag{26}$$

For both variants it is taken that for $K_J \le K_{\min}$ the brittle fracture probability $P_f = 0$.

These two variants differ by the physical meaning. Equation (25) corresponds to situation when for $K_J > K_{\min}$ the whole plastic zone volume near the crack tip is taken as the working volume**. Equation (26) corresponds to situation when the working volume (for $K_J > K_{\min}$) is calculated as the difference of the whole plastic zone volume at K_J and the plastic zone volume at $K_{\min}$. By other words, the plastic zone corresponding to $K_{\min}$ does not contribute to the brittle fracture probability for $K_J > K_{\min}$.

Choice of the first or second variants may be formal or may be based on the probabilistic model of brittle fracture.

According to the Prometey model $P_f = 0$ if $\sigma_{nuc} \le \sigma_{d0}$ or $r_p \le \rho_{uc}$ and $P_f > 0$ if $\sigma_{nuc} > \sigma_{d0}$ and $r_p > \rho_{uc}$, where r_p is the plastic zone size and ρ_{uc} is the unit cell size.

From the physical viewpoint the unit cell size ρ_{uc} is determined by distance between barriers for dislocations. Therefore only when $r_p > \rho_{uc}$ the dislocation pile-ups generating cleavage microcracks may form [54]. Hence, conditions $\sigma_{nuc} \le \sigma_{d0}$ and $r_p \le \rho_{uc}$ mean that the microcrack nucleation condition (13a) is not met in the unit cell nearest to the crack tip. These conditions allow the calculation of the parameter $K_{\min}$ with the Prometey model [55] so that when $K_J \le K_{\min}$, we have $P_f = 0$.

Thus according to the Prometey model the unit cell nearest to the crack tip does not contribute to the fracture probability only when $K_J \le K_{\min}$. For the case when $K_J > K_{\min}$ the above zone contributes to the fracture probability. It means that the fracture probability P_f is calculated with Eq. (25) but not with Eq. (26). So, according to the Prometey model $P_f \sim B(K_I - K_{\min})^4$. Therefore the critical remark in [6] on this issue is not correct. It has been stated in [6] that it follows from the Prometey model that

** The working volume is defined as material volume that contributes to the fracture probability.

$$P_f = 1 - \exp\left[-\left(\frac{K_{JC}^4 - K_{\min}^4}{K_0^4 - K_{\min}^4}\right)\right], \tag{27}$$

that is in contradiction with Eq. (8) used in the UC. The above explanation has shown that this statement is mistaken.

At the last point it is necessary to return to an issue of application of the MC and UC for RPV structural integrity assessment.

The performed comparison has shown that for low values of T_0 both methods provide practically the same prediction of the $K_{JC}(T)$ curves. At the same time with increasing T_0 the UC predicts $K_{JC}(T)$ curve more adequately than the MC, at least, when CT specimens with thickness of 12.5 mm and more are tested.

For PCC specimens in same cases the MC may provide better prediction than the UC that is connected with the known particularities of fracture for PCC specimens. These specimens loose the strain constraint with increasing load significantly earlier than CT specimens and, as a result, $K_{JC}(T)$ curve for PCC specimens is steeper than the curve for CT specimens [25–27, 56].

Taking into account that the stress-and-strain fields near the tip of postulated crack in RPV are closer to the fields near the crack tip for CT specimens, the following conclusion may be drawn when assessing RPV structural integrity.

RPV integrity assessment on the basis of direct application of $K_{JC}(T)$ curve predicted by the UC method is more adequate than when using the MC. Direct application of the MC may give non-conservative assessment of RPV structural integrity.

The MC may provide conservative assessment of RPV service life only if RPV structural integrity is estimated with the ASME K_{JC} reference curve indexed to reference temperature RT_{T0} which is defined as $RT_{T0} = T_0 + 35^\circ\text{F}$ according to the ASME Code Case 629 [57].

Conclusions

1. Three statistical parameters (L, δ, and σ) have been used for quantitative comparison of the Master Curve and Unified Curve by treatment of the fracture toughness data base consisting of 44 sets for ferritic materials with various degrees of embrittlement. It has been shown that all the statistical parameters provide similar results when comparing the MC and UC. This treatment has shown the advantage of the UC over the MC when using any statistical parameters (L, δ, and σ).

2. The main requirements have been formulated for objective comparison of the MC and UC. Taking into account that the main difference between these methods consists exactly in the description of the $K_{JC}(T)$ curve shape these requirements are formulated as follows.

2.1. Fracture toughness data for PCC (SE(B)-10 mm) specimens should not be used as the $K_{JC}(T)$ curve for PCC specimens differs from the curve for standardized CT specimens. The $K_{JC}(T)$ curve for PCC specimens is steeper than the curve for CT specimens.

2.2. The number of incorrect results in the fracture toughness data set should be sufficiently small as for most cases of incorrect results J-integral does not control the stress-and-strain fields near a crack tip and, as a result, incorrect results damage the standard distribution on K_{JC}.

2.3. When using the parameter L for comparison of the MC and UC, it is advisable to take the same K_{JC}^{shelf} level for both methods, for example, $K_{JC}^{shelf} = 30$ MPa$\sqrt{\text{m}}$. This requirement is caused by a large contribution of K_{JC} values near the low shelf in the parameter L and a weak influence of these values on the $K_{JC}(T)$ curve shape.

3. The data sets have in detail been analyzed for which definite advantage of the MC over the UC has been declared according to [6]. Possible reasons for quite different and contradictory conclusions in the present research and in [6] have been revealed. These reasons are mainly connected with violation of the above requirements for objective comparison of the MC and UC.

For some sets a seeming advantage of the MC revealed in [6] is caused by overestimated K_{JC} values near the low shelf and the known difference in the K_{JC}^{shelf} values for the MC and UC but not a difference in the $K_{JC}(T)$ curve shape.

For other cases the conclusion about the advantage of the MC is based on the data sets from PCC specimens as clearly seen from Fig. 2.

Therefore comparison of the MC and UC in [6] cannot be considered as objective.

4. The main properties of the $K_{JC}(T)$ dependences for ferritic steels and their transformation for embrittled conditions have been analyzed on the basis of the Prometey probabilistic brittle fracture model and experimental data.

It has been shown that for low T_0 values the transformation of the $K_{JC}(T)$ curve is described by the lateral temperature shift and its shape is practically controlled by the temperature dependence of the thermal component $\sigma_{Ys}(T)$ of the yield stress. It has been found from the test results that for many ferritic steels the dependences $\sigma_{Ys}(T)$ may be approximated by the same exponential function. These facts explain why the $K_{JC}(T)$ dependences for different ferritic steels with small degrees of embrittlement may be approximated by the same function taken for the MC. When comparing the values of the parameter $\gamma = 0.019$ determining the MC shape and the constant h determining the $\sigma_{Ys}(T)$ dependence the correlation has been found as $\gamma \approx 2h$.

It has been explained with the local brittle fracture criterion used in the Prometey model why the $K_{JC}(T)$ curves change their shapes when degree of embrittlement increases significantly that is in agreement with most experimental data sets from CT specimens.

5. Prediction of $K_{JC}(T)$ curve used for RPV structural integrity assessment has to be performed with account taken of variation of $K_{JC}(T)$ curve shape if (i) the temperature range for RPV integrity assessment does not coincide with the temperature range for small-size specimen testing, and (ii) the ASME K_{JC} reference curve is not used. Then the use of the Unified Curve method may be recommended.

Р е з ю м е

Проаналізовано два інженерних метода – Master Curve і Unified Curve стосовно оцінки опору крихкому руйнуванню корпусів реакторів. Для порівняння цих методів при обробці бази даних значень в'язкості руйнування для 44 сталей та їх швів із різним ступенем окрихчення було використано три різних статистичних параметра. Установлено, що метод Unified Curve має переваги перед методом Master Curve. Проаналізовано можливі причини гаданої переваги методу Master Curve та сформульовано й обґрунтовано вимоги щодо об'єктивного порівняння методів. Узагальнення експериментальних даних щодо температурної залежності термоактивованої частини границі плинності і моделі Prometey (моделі крихкого руйнування, що базується на локальному підході) дозволило пояснити, чого залежність $K_{JC}(T)$ для різних сталей, за незначного ступеня окрихчення, може бути апроксимована експоненціальною функцією, зокрема залежністю Master Curve. Отримано кореляцію між температурною залежністю термоактивованої частини границі плинності і залежністю Master Curve.

1. *ASTM E 1921-13. Standard Test Method for Determination of Reference Temperature, T_0, for Ferritic Steels in the Transition Range*, Annual Book of ASTM Standards, West Conshohocken, PA (2013).

2. J. G. Merkle, K. Wallin, and D. E. McCabe, *Technical Basis for an ASTM Standard on Determining the Reference Temperature, T_0, for Ferritic Steels in the Transition Range*, NUREG/CR-5504, ORNL/TM-13631 (1998).
3. B. Z. Margolin, A. G. Gulenko, V. A. Nikolaev, and L. N. Ryadkov, "A new engineering method for prediction of the fracture toughness temperature dependence for RPV steels," *Int. J. Press. Vess. Piping*, **80**, 817–829 (2003).
4. B. Margolin, B. Gurovich, V. Fomenko, et al., "Fracture toughness prediction for highly irradiated RPV materials: From test results to RPV integrity assessment," *J. Nucl. Mater.*, **432**, 313–322 (2013).
5. G. A. Korn and T. M. Korn, *Mathematical Handbook for Scientists and Engineers*, McGraw-Hill Book Company, New York–San Francisco–London (1968).
6. K. Wallin, "Objective comparison of the Unified Curve and Master Curve methods," *Int. J. Press. Vess. Piping*, **122**, 31–40 (2014).
7. K. Wallin, "The scatter in K_{Ic} results," *Eng. Fract. Mech*., **19**, 1085–1093 (1984).
8. K. Wallin K, "The size effect in K_{Ic} results," *Eng. Fract. Mech.*, **22**, 149–163 (1985).
9. F. M. Beremin, A. Pineau, F. Mudry, et al., "A local criterion for cleavage fracture of a nuclear pressure vessel steel," *Met. Trans. A*, **14**, 2277–2287 (1983).
10. B. Z. Margolin, A. G. Gulenko, and V. A. Shvetsova, "Probabilistic model for fracture toughness prediction based on the new local fracture criteria," *Int. J. Press. Vess. Piping*, **75**, 307–320 (1998).
11. K. Wallin, "Introduction to the Master Curve approach and ASTM E 1921," in: *Use and Applications of the Master Curve for Determining Fracture Toughness* (Workshop MASC 2002), Helsinki–Stockholm (2002), pp. 4.1–4.17.
12. K. Wallin, *Recommendations for the Application of Fracture Toughness Data for Structural Integrity Assessments*, NUREG/CR-0131, ORNL/TM-12413 (1993).
13. B. Z. Margolin, G. P. Karzov, V. A. Shvetsova, et al., "Application of local approach concept of cleavage fracture to VVER materials," in: *Service Experience and Failure Assessment Applications* (The 2002 ASME Pressure Vessels and Piping Conference, August 2002, Vancouver), Vol. 437 (2002), pp. 113–120.
14. B. Z. Margolin, V. A. Shvetsova, A. G. Gulenko, and A. V. Ilyin, "Cleavage fracture toughness for 3Cr-Ni-Mo-V reactor pressure vessel steel. Theoretical prediction and experimental investigation," *Int. J. Press. Vess. Piping*, **78**, 715–729 (2001).
15. D. E. McCabe, "Irradiation effect on engineering materials," in: *Heavy-Section Steel Irradiation Program* (Progress Report for April 1997-March 1998), NUREG/CR-5591, ORNL/TM-11568, Vol. 8, No. 2, U.S. Nuclear Regulatory Commission, Washington, DC (2000), pp. 2-1–2-7.
16. R. K. Nanstad, D. E. McCabe, B. H. Menke, et al., "Effects of radiation on K_{Ic} curves for high-copper welds," in: *Effects of Radiation on Materials*: 14th Int. Symp., N. Packan, R. Stoller, and A. Kumar (Eds.), ASTM STP 1046, Philadelphia, PA (1990), pp. 214–233.
17. J. G. Merkle, K. Wallin, and D. E. McCabe, *Technical Basis for an ASTM Standard on Determining the Reference Temperature, T_0, for Ferritic Steels in the Transition Range*, NUREG/CR-5504, ORNL/TM-13631 (1999).
18. K. Wallin, "Master Curve approach and SI assessment," in: *Use and Applications of the Master Curve for Determining Fracture Toughness* (Workshop MASC 2002), Helsinki–Stockholm (2002), pp. 8.1–8.19.

19. E. Keim, R. Bartsch, and G. Nagel, "Application in licensing West European reactor," in: *Use and Applications of the Master Curve for Determining Fracture Toughness* (Workshop MASC 2002), Helsinki–Stockholm (2002), pp. 10-1–10-30.

20. S. R. Ortner, "Outstanding issues in Master Curve applications," in: *Use and Applications of the Master Curve for Determining Fracture Toughness* (Workshop MASC 2002), Helsinki–Stockholm (2002), pp. 19.1–19.14.

21. B. Z. Margolin, V. A. Shvetsova, A. G. Gulenko, et al., "Fracture toughness predictions for a reactor pressure vessel steel in the initial and highly embrittled states with the Master Curve approach and a probabilistic model," *Int. J. Press. Vess. Piping*, **79**, 219–231 (2002).

22. M. A. Sokolov, R. K. Nanstad, and M. K. Miller, "Fracture toughness characterization of a highly embrittled RPV weld," in: M. Grossbeck (Ed.), *Effects of Radiation on Materials*, ASTM STP 1447, West Conshohocken, PA (2003), pp. 123–137.

23. T. Planman, H. Keinanen, K. Wallin, and R. Rintamaa, "Master Curve analysis of highly embrittled pressure vessel steel," in: *Irradiation Embrittlement and Mitigation* (Proc. of the IAEA Specialists Meeting in Gloucester, UK, 2001), IAEA TWG-LMNPP-01/2 (2002), pp. 521–535.

24. *Master Curve Approach to Monitor Fracture Toughness of Reactor Pressure Vessel in Nuclear Power Plants*, IAEA-TECDOC-1631, IAEA, Vienna (2009).

25. J. Heerens, D. Hellmann, and R. A. Ainsworth, "Fracture toughness determination in the ductile-to-brittle transition regime – pre-cracked Charpy specimens compared with standardized compact specimens," in: A. Pineau and D. Francois (Eds.), *From Charpy to Present Impact Testing* (Proc. of CCC, October 2001), Poitiers, France (2001), pp. 297–305.

26. J. Heerens, R. A. Ainsworth, R. Moskovic, and K. Wallin, "Fracture toughness characterization in the ductile-to-brittle transition and upper shelf regimes using pre-cracked Charpy single-edge bend specimens," *Int. J. Press. Vess. Piping*, **82**, 649–667 (2005).

27. D. Lidbury et al., "Recent R&D on constraint based fracture mechanics: the Vocalist and NESC–IV projects," in: Proc. of Int. Sem. on *Transferability of Fracture Toughness Data for Integrity of Ferritic Steel Component* (November 17–18, 2004, Petten, the Netherlands), Luxemburg (2004), pp. 38–58.

28. B. Margolin, V. Nikolaev, V. Fomenko, and L. Ryadkov, "Modification of pre-cracked Charpy specimens for surveillance specimen programs," in: Proc. of ASME 2009 PVP Conference (July 26–30, 2009, Prague), Paper No. PVP2009-77096 (2009), pp. 59–69.

29. V. A. Nikolaev, B. Z. Margolin, L. N. Ryadkov, and V. N. Fomenko, "Analysis of applicability of small-sized specimens to prediction of temperature dependence of fracture toughness," *Strength Mater.*, **41**, No. 2, 119–134 (2009).

30. D. E. McCabe, R. K. Nanstad, S. K. Iskander, et al., *Evaluation of WF-70 Weld Metal From the Midland Unit 1 Reactor Vessel*, NUREG/CR-5736, Oak Ridge, TN (2000).

31. J. A. Begley and P. R. Toolin, "Fracture toughness and fatigue crack growth rate properties of a Ni-Cr-Mo-V steel sensitive to temper embrittlement," *Int. J. Fract.*, **9**, 243–253 (1973).

32. S. Ishino, T. Kawakami, T. Hidaka, and M. Satoh, "The effect of chemical composition on irradiation embrittlement," in: Proc. of the 14th MPA-Seminar on *Safety and Reliability of Plant Technology: Long-Term Integrity of Pressure Components of Nuclear Power Plants* (Oct. 6–7, 1988, Stuttgart), Vol. 1 (1988), pp. 13.1–13.16.

33. H. D. Greenberg, E. T. Wessel, and W. H. Pryle, "Fracture toughness of turbine-generator rotor forgings," *Eng. Fract. Mech.*, **1**, 653–674 (1970).
34. C. J. Bolton, P. J. E. Bischler, M. R. Wootton, et al., "Fracture toughness of weld metal samples removed from a decommissioned Magnox reactor pressure vessel," *Int. J. Press. Vess. Piping*, **79**, 685–692 (2002).
35. B. Z. Margolin and V. A. Shvetsova, "Brittle fracture criterion: structural mechanics approach," *Strength Mater.*, **24**, No. 2, 115–131 (1992).
36. B. Z. Margolin and V. A. Shvetsova, "Local criterion for cleavage fracture: structural and mechanical approach," *J. Physique IV*, **6**, C6-225–C6-234 (1996).
37. B. Z. Margolin, V. A. Shvetsova, and G. P. Karzov, "Brittle fracture of nuclear pressure vessel steels. Part I. Local criterion for cleavage fracture," *Int. J. Press. Vess. Piping*, **72**, 73–87 (1997).
38. B. Z. Margolin, A. G. Gulenko, and V. A. Shvetsova, "Improved probabilistic model for fracture toughness prediction for nuclear pressure vessel steels," *Int. J. Press. Vess. Piping*, **75**, 843–855 (1998).
39. B. Z. Margolin, V. A. Shvetsova, A. G. Gulenko, and V. I. Kostylev, "Application of a new cleavage fracture criterion for fracture toughness prediction for RPV steels," *Fatigue Fract. Eng. Mater. Struct.*, **29**, No. 9, 697–713 (2006).
40. B. Z. Margolin, V. A. Shvetsova, A. G. Gulenko, and V. I. Kostylev, "Prometey local approach to brittle fracture: development and application," *Eng. Fract. Mech.*, **75**, 3483–3498 (2008).
41. B. Z. Margolin, V. I. Kostylev, and E. Keim, "Prediction of brittle fracture under complex loading on the basis of a local probabilistic approach," *Int. J. Press. Vess. Piping*, **81**, 949–959 (2004).
42. B. Z. Margolin, V. I. Kostylev, and A. I. Minkin, "The effect of ductile crack growth on the temperature dependence of cleavage fracture toughness for a RPV steel with various degrees of embrittlement," *Int. J. Press. Vess. Piping*, **80**, 285–296 (2003).
43. B. Z. Margolin and V. I. Kostylev, "Analysis of biaxial loading effect on fracture toughness of reactor pressure steels," *Int. J. Press. Vess. Piping*, **75**, 589–601 (1998).
44. B. Margolin, V. Shvetsova, and A. Gulenko, "Radiation embrittlement modelling in multi-scale approach to brittle fracture of RPV steels," *Int. J. Fract.*, **179**, 87–108 (2013).
45. R. Berner and H. Kronmüller, *Plastische Verformung von Einkristallen*, Springer-Verlag, Berlin–Heidelberg (1965).
46. C. W. Hunter and J. A. Williams, "Fracture and tensile behavior of neutron-irradiated A533-B pressure vessel steel," *Nucl. Eng. Des.*, **17**, 131–148 (1971).
47. J. J. McGowan, R. K. Nanstad, and K. R. Thoms, *Characterization of Irradiated Current-Practice Welds and A533 Grade B Class 1 Plate for Nuclear Pressure Vessel Steel*, NUREG/CR-4880, Vol. 1, ORNL-6484/V1, Oak Ridge, TN (1988).
48. *Reference Manual on the IAEA JRQ Correction Monitor Steel for Irradiation Damage Studies*, IAEA-TECDOC-1230, ISSN 1011-4289, IAEA, Vienna (2001).
49. A. F. Yoffe, M. V. Kirpicheva, and M. A. Levitskay, "Deformation and strength of crystals," *Zh. Russ. Phys.-Chim. Obshch.*, **56**, 489–504 (1924).
50. N. N. Davidenkov, *Dynamic Testing of Materials* [in Russian], ONTI, Moscow (1936).
51. Y. B. Fridman, *Mechanical Properties of Metals* [in Russian], Oborongiz, Moscow (1952).

52. G. S. Pisarenko and A. Y. Krasowsky, “Analysis of kinetics of quasibrittle fracture of crystalline materials,” in: Proc. Int. Conf. on *Mechanical Behaviour of Materials* (Kyoto, 1971), Vol. I, Kyoto (1972), pp. 421–432.

53. R. O. Ritchie, J. F. Knott, and J. R. Rice, “On the relation between critical tensile stress and fracture toughness in mild steel,” *J. Mech. Phys. Solids*, **21**, 395–410 (1973).

54. B. Z. Margolin and G. P. Karzov, “Fatigue failure of nuclear pressure vessel steels. II. Prediction of fatigue crack propagation,” *Int. J. Press. Vess. Piping*, **74**, 111–120 (1997).

55. V. A. Shvetsova, B. Z. Margolin, and A. G. Gulenko, “Stress-controlled and stress-and-strain controlled criteria of brittle fracture in local approach,” in: Proc. of 13th Int. Conf. on Fracture (June 16–21, 2013, Beijing, China), Beijing (2013), pp. 5559–5568.

56. L. Stumpfrock, “Constraint modified fracture toughness specimens,” in: Proc. of Int. Sem. on *Transferability of Fracture Toughness Data for Integrity of Ferritic Steel Component* (November 17–18, 2004, Petten, the Netherlands), Luxemburg (2004), pp. 59–74.

57. *ASME Code Case 629*, IAEA Technical Reports Series No. 429 (2005).

Received 08. 02. 2016